Effects of vegetation canopy processes on snow surface energy and mass balances

Guo-Yue Niu and Zong-Liang Yang

Department of Geological Sciences, John A. and Katherine G. Jackson School of Geosciences, University of Texas at Austin, Austin, Texas, USA

Received 8 April 2004; revised 28 June 2004; accepted 29 September 2004; published 11 December 2004.

[1] This paper addresses the effects of canopy physical processes on snow mass and energy balances in boreal ecosystems. We incorporate new parameterizations of radiation transfer through the vegetation canopy, interception of snow by the vegetation canopy, and under-canopy sensible heat transfer processes into the Versatile Integrator of Surface and Atmosphere (VISA) and test the model results against the Boreal Ecosystem-Atmosphere Study (BOREAS) data observed at South Study Area, Old Jack Pine. A modified two-stream radiation transfer scheme that accounts for the three-dimensional geometry of vegetation accurately simulates the transferring of solar radiation through the vegetation canopy when the leaf and stem area index is reduced to match the observed. VISA produces higher-than-observed surface albedo in wintertime. Implementation of a snow interception model that explicitly describes the loading and unloading of snow and the melting and refreezing of snow on the canopy into VISA reduces the fractional snow cover on the canopy and the surface albedo. VISA overestimates the downward sensible heat fluxes from the canopy to the snow surface, which leads to earlier snow ablation and a shallower snowpack than the observed. Explicitly including a canopy heat storage term in the canopy energy balance equation decreases the spuriously large amplitude of the diurnal canopy temperature variation and reduces the excessive daytime sensible heat flux from the canopy downward to the snow surface. Sensitivity tests reveal that the turbulent sensible heat flux below the vegetation canopy strongly depends on the canopy absorption coefficient of momentum. During spring the daytime temperature difference between the snow surface and the vegetation canopy forms a strongly stable atmospheric condition, which results in a larger absorption coefficient of momentum and a weak turbulent sensible heat flux. The modeled excessive downward sensible heat flux from the vegetation canopy to the snow surface is considerably reduced through the stability correction to the canopy absorption coefficient of momentum. *INDEX TERMS:* 1863 Hydrology: Snow and ice (1827); 3307 Meteorology and Atmospheric Dynamics: Boundary layer processes; 3322 Meteorology and Atmospheric Dynamics: Land/atmosphere interactions; 3359 Meteorology and Atmospheric Dynamics: Radiative processes; 3379 Meteorology and Atmospheric Dynamics: Turbulence; *KEYWORDS:* vegetation canopy, snow interception, radiation transfer

Citation: Niu, G.-Y., and Z.-L. Yang (2004), Effects of vegetation canopy processes on snow surface energy and mass balances, *J. Geophys. Res.*, *109*, D23111, doi:10.1029/2004JD004884.

1. Introduction

[2] Snow cover is an important part of the climate system because of its high albedo, low thermal conductivity, and ability to absorb heat when melting. In addition, the snowmelt-induced runoff is the primary source of stream flow and groundwater recharge in cold and alpine regions. The impacts of snow-cover processes on global and regional climate have been investigated by numerous researchers [*Yeh et al.*, 1983; *Walsh and Ross*, 1988; *Barnett et al.*, 1989; *Cess et al.*, 1991; *Randall et al.*, 1994] using general circulation models (GCMs). The representation of snow processes in soil vegetation-atmosphere transfer schemes (SVATs) for use in GCMs was relatively simple [*Verseghy*, 1991; *Bonan*, 1996; *Yang et al.*, 1997; *Douville et al.*, 1995]. Recently, several new parameterizations of snow for use in SVATs have improved the representation of the internal processes of snowpack such as densification and multiphase changes of water [*Loth et al.*, 1993; *Lynch-Stieglitz*, 1994; *Sun et al.*, 1999; *Dai et al.*, 2003; *Yang and Niu*, 2003; *Xue et al.*, 2003]. Most of these developments in the representation of snowpack are simplified from schemes with detailed internal processes such as grain-size growth and gravitational flows of liquid water within a snowpack [e.g., *Anderson*, 1976; *Jordan*, 1991; *Brun et al.*, 1992]. These new snow schemes have been tested mainly with field data from open, unvegetated areas. There has been an

0148-0227/04/2004JD004884$09.00

increasing awareness that snowpack modeling for hydrological applications and climate studies needs to account for the radiative effects of the vegetation canopy [*Hardy et al.*, 1997; *Davis et al.*, 1997; *Link and Marks*, 1999] and the impacts of the interception of snow by the vegetation canopy [*Storck and Lettenmaier*, 2000; *Essery et al.*, 2003; *Gusev and Nasonova*, 2003].

[3] Forest canopies dramatically modify the snow mass and energy balances by affecting the radiation transfer, snowfall interception, and wind regime. A number of sensitivity studies using GCMs have found that the removal of all forests north of 45°N would lead to cooling and delayed snowmelt because of the increased surface albedo [*Thomas and Rowntree*, 1992; *Bonan et al.*, 1992; *Chalita and Treut*, 1994; *Douville and Royer*, 1997]. Therefore a simple and robust parameterization of the radiation transfer through the canopy, the interception of snow by the canopy, and the under-canopy turbulent transfer processes is required in order to obtain realistic simulations.

[4] SVATs usually use a two-stream approximation scheme [*Dickinson*, 1983; *Sellers*, 1985] for radiation transfer in the canopy [*Sellers et al.*, 1986; *Bonan*, 1996; *Bonan et al.*, 2002]. The two-stream approximation is efficient computationally, but neglects heterogeneity within a vegetation type (i.e., the clumpings and gaps associated with boreal forests). Complicated radiation-transfer models that explicitly account for canopy geometry are available (e.g., the Geometric-Optical and Radiative Transfer (GORT) model [*Li et al.*, 1995; *Ni et al.*, 1997]), but they may be too computationally expensive for use in GCMs. Efforts have been made to develop simplified approaches to predict radiation transfer through the canopy [*Nijssen and Lettenmaier*, 1999; *Yang et al.*, 2001]. *Yang et al.* [2001] have modified a two-stream canopy transfer model by introducing an explicit representation of vegetation canopy geometry; their simulation produced results comparable to those simulated by GORT.

[5] Interception of snowfall by the vegetation canopy significantly reduces snow mass on the forest floor. About 30–40% of the annual snowfall over complete coniferous canopies sublimates from the canopy and thus never reaches the ground [*Schmidt and Gluns*, 1991; *Pomeroy and Schmidt*, 1993; *Hedstrom and Pomeroy*, 1998; *Storck and Lettenmaier*, 2000]. Depending on meteorological conditions, the intercepted snow may fall to the ground, sublimate, melt or refreeze. Most recently, *Essery et al.* [2003] improved their snowpack simulations by implementing a snowfall interception model and revising the representation of sublimation of the canopy-intercepted snow. However, most other SVATs do not explicitly distinguish between solid and liquid phases of water on the canopy surface, and they use the same interception capacity for both snowfall and rainfall.

[6] The turbulence in vegetation canopies has been a subject of active research in recent years [*Raupach et al.*, 1996; *Katul and Albertson*, 1998; *Shaw and Patton*, 2003; *Poggi et al.*, 2004]. Underlying the classical constant-flux surface layer, the canopy layer may have three sublayers: (1) the canopy roughness sublayer, where momentum is mainly reduced by the form drag of the canopy roughness elements through wake effects, (2) the within-canopy sublayer, where the momentum is mainly reduced by viscous drag, and (3) the under-canopy sublayer, where the flow may be dominated by von Karman streets. Under the assumption of the exponential decay of the eddy diffusivity in the under-canopy sublayer, the turbulent transfer of momentum and heat strongly depends on the decay factor, the absorption coefficient of momentum, which is a function of the atmospheric stability below the canopy and the density, height, and type of vegetation [*Goudriaan*, 1977; *Brutsaert*, 1982; *Shuttleworth and Wallace*, 1985; *Choudury and Monteith*, 1988]. During the snow-melting season, the daytime canopy temperature is always several degrees above the snow surface temperature, which is at or below the freezing point. As a result, an unstable above-canopy surface layer and a stable under-canopy sublayer may be formed. The under-canopy turbulent transfer of momentum and heat is strongly suppressed by the stable atmospheric condition [*Storck and Lettenmaier*, 2000].

[7] The goal of this paper is to use the VISA [*Yang and Niu*, 2003] to address the effects that the radiation transfer through the vegetation canopy, the interception of snow by the vegetation canopy, and the turbulent transfer of sensible heat have on the snow mass and energy balances. We first describe our modifications to the schemes of radiation transfer, snow interception, and turbulent transfer and then assess the validity of these new schemes. We also examine the effect that introducing a canopy (including the canopy-intercepted water) heat capacity into the vegetation canopy energy balance equation has on the simulation of the surface temperature and snowmelt. We conduct a series of simulation runs to assess the sensitivity of under-canopy sensible heat fluxes to the canopy absorption coefficient of momentum. We use the BOREAS SSA-OJP and the Oregon data sets [*Storck et al.*, 2002] to validate these new parameterization schemes.

2. Versatile Integrator of Surface Atmosphere Processes

[8] The VISA model [*Yang and Niu*, 2003] integrates recent developments in the representation of snow, runoff and vegetation growth into the National Center for Atmospheric Research Land Surface Model version 1.0 (NCAR LSM1.0) [*Bonan*, 1996]. Because this study focuses on the snow mass and energy balances in the presence of the vegetation canopy, VISA retains the multilayer snow scheme described in the work of *Yang and Niu* [2003] but excludes the vegetation growth scheme.

2.1. A Modified Two-Stream Radiation-Transfer Scheme

[9] The two-stream approximation used in the default version of VISA to calculate the radiation transfer through the vegetation canopy is modified in this study following *Yang et al.* [2001] and *Yang and Friedl* [2003] to explicitly include the 3-D structure of the vegetation canopy (Figure 1a). The total canopy gap probability (the chance that a photon penetrates through the vegetation without being intercepted by any crowns), P_c, is given by the sum of the between-crown gap probability, P_{bc}, which is a function of crown geometric properties and the solar zenith angle, and the within-crown gap probability, P_{wc},

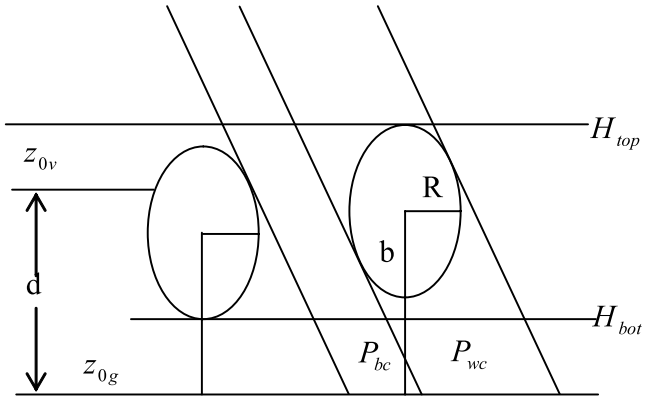

Figure 1a. Schematic diagram of the vegetation canopy structure.

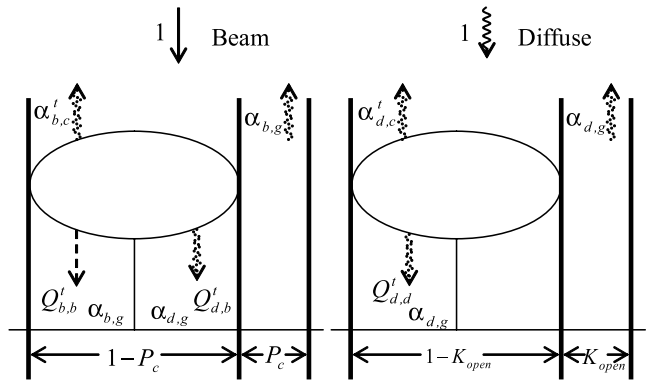

Figure 1b. Schematic diagram of the modified two-stream radiation transfer. The straight lines stand for beam; the curves stand for diffuse radiation.

which is parameterized on the basis of a modified version of Beer's law:

$$P_{bc} = e^{-\rho_t \pi R^2 / \cos(\theta')}, \tag{1}$$

$$P_{wc} = (1 - P_{bc}) e^{-0.5 F_a H_d / \cos\theta}, \tag{2}$$

$$K_{open} = \int_0^{\pi/2} P_{bc} \sin(2\theta) d\theta, \tag{3}$$

where ρ_t is the crown density (stems/m^2), R is the horizontal crown radius, $\theta' = \tan^{-1}[(b/R)\tan(\theta)]$, b is the vertical crown radius, and θ is the solar zenith angle. K_{open} is the between-crown gap probability for diffuse radiation, H_d is the crown depth ($H_d = H_{top} - H_{bot}$, where H_{top} and H_{bot} are the top and bottom heights of the crown). F_a is the foliage area volume density (m^{-1}), which is equal to $LSAI/(\frac{4}{3}\pi R^2 b \rho_t)$, where $LSAI$ is the effective leaf and stem area index, through which the effect of clumping of needles into shoots is included [*Chen et al.*, 1991].

[10] The radiative fluxes derived from a two-stream radiation-transfer scheme can be modified by implementing the total canopy gap probability, $P_c (= P_{bc} + P_{wc})$. Thus the snow surface received direct beam fluxes, $Q_{b,b}$ (Figure 1b), per unit incident direct beam is

$$Q_{b,b} = Q^t_{b,b}(1 - P_c) + P_c. \tag{4}$$

The snow surface received diffuse fluxes per unit incident direct beam and diffuse radiation, $Q_{d,b}$ and $Q_{d,d}$ (Figure 1b), are

$$Q_{d,b} = Q^t_{d,b}(1 - P_c), \tag{5}$$

$$Q_{d,d} = Q^t_{d,d}(1 - K_{open}) + K_{open}. \tag{6}$$

The upward diffuse fluxes per unit incident direct beam and diffuse fluxes (i.e., the surface albedos), $\alpha_{d,b}$ and $\alpha_{d,d}$ (Figure 1b), are

$$\alpha_{d,b} = \alpha^t_{b,c}(1 - P_c) + \alpha_{b,g} P_c, \tag{7}$$

$$\alpha_{d,d} = \alpha^t_{d,c}(1 - K_{open}) + \alpha_{d,g} K_{open}. \tag{8}$$

[11] The variables with superscript t in equations (4)–(8) are calculated from a two-stream radiation transfer model. The subscripts b and d stand for direct beam and diffuse radiations, respectively; the subscript c stands for the canopy. The $\alpha_{b,g}$ and $\alpha_{d,g}$ are ground surface albedos for direct beam and diffuse radiations. Note that in equation (5), the direct beam in P_c cannot be scattered by the vegetation canopy because it directly penetrates through the vegetation canopy. The optical parameters, such as scattering coefficient and the upscatter parameters for diffuse radiation and direct beam, which vary with wavelength, are averages of those for snow and vegetation weighted respectively by the fractional canopy-intercepted snow, f_{sno}, and the canopy fraction, $(1 - f_{sno})$, as described in the work of *Bonan* [1996] and *Sellers et al.* [1986]. The geometry parameters for SSA-OJP (represented in VISA as an evergreen needleleaf tree) are listed in Table 1.

[12] Figure 2 shows the surface albedo and canopy transmittance as a function of LSAI calculated from the two-stream and the modified two-stream schemes for needleleaf trees. The surface albedos for vegetated surfaces covered by intercepted snow ($f_{sno} = 1$) are significantly higher than those for vegetated surfaces not covered by intercepted snow ($f_{sno} = 0$). As the LSAI increases, more underlying snow is masked, and the surface albedo decreases. When the gap probabilities are taken into consideration, the simulated surface albedo and the canopy transmittance increase. The influence of canopy gap probabilities strongly depends on the cosine of the solar zenith angle as shown in Figure 3. Because the cosine of the solar zenith angle is given as its maximum value ($\mu = 1.0$), the differences between the default two-stream scheme and the modified two-stream scheme shown in Figure 2 represent the maximum influence that the modified scheme

Table 1. Geometry Parameters for SSA-OJP

Variable	SSA-OJP
H_{top} (m)	16.2
H_{bot} (m)	4.2
R (m)	1.2
b(m)	3.5
ρ_t (m^{-2})	0.284
LSAI	1.89

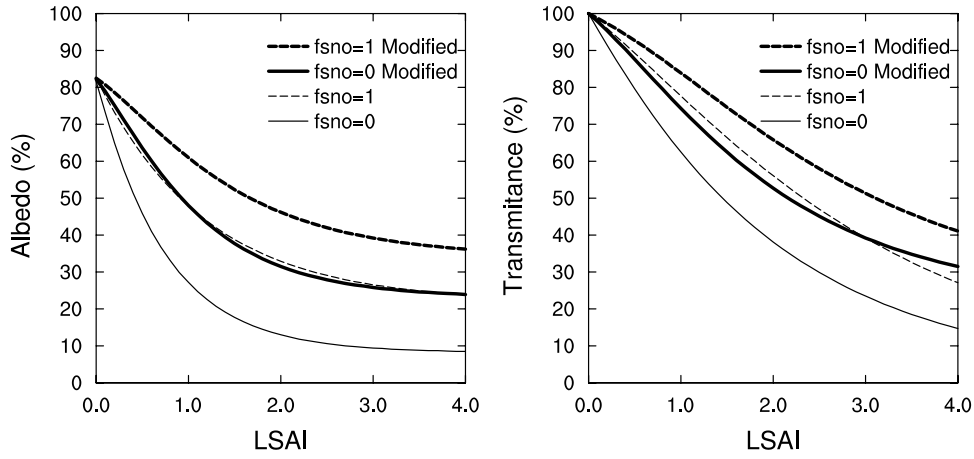

Figure 2. Surface albedo and canopy transmittance as a function of LSAI for needleleaf evergreen trees with $\chi_L = 0.01$, where χ_L is the departure of leaf angles from a random distribution (1 for horizontal leaves, 0 for random leaves, and -1 for vertical leaves). In the calculations the optical parameters are identical to those in the NCAR LSM1.0, and the cosine of the solar zenith angle $\mu = 1.0$. The ground is covered by fresh snow with albedos for the visible band at 0.95 and albedos for the near-infrared at 0.70. Thin lines are for the two-stream model, and the thick lines are for the modified two-stream model. Solid lines represent $f_{sno} = 0$, and dashed lines represent $f_{sno} = 1$.

can have on the calculation of the surface albedo and canopy transmittance.

2.2. A Snow-Interception Model

[13] The newly introduced snow-interception model allows for both liquid water and ice to be present on the vegetation canopy. The canopy liquid water balance may be written:

$$\frac{\partial M_{liq}}{\partial t} = R_{intr} + (R_{dew} - R_{eva}) + \left(R_{melt} - R_{frz}\right), \tag{9}$$

where M_{liq} (kg m^{-2}) is the storage of water at the canopy surface, and R_{intr}, R_{dew}, and R_{eva} are interception rate for rain, dew rate, and evaporation rate [*Bonan*, 1996]. R_{melt} and R_{frz} are melting and refreezing rates, which will be described below.

[14] The canopy ice balance is:

$$\frac{\partial M_{ice}}{\partial t} = (R_{load} - R_{unload}) + \left(R_{frost} - R_{sub}\right) + \left(R_{frz} - R_{melt}\right), \tag{10}$$

where M_{ice} (kg m^{-2}) is the storage of ice at the canopy surface and R_{load} (kg m^{-2} s^{-1}) and R_{unload} (kg m^{-2} s^{-1}) are snow loading and unloading rates. R_{frost} and R_{sub} are frost and sublimation rate [*Bonan*, 1996]. Following *Hedstrom and Pomeroy* [1998]:

$$R_{load} = \left(M_{ice,\max} - M_{ice}\right)\left(1 - e^{-P_s \Delta t / M_{ice,\max}}\right)/\Delta t, \tag{11}$$

where Δt is the time step. P_s (kg m^{-2} s^{-1}) and $M_{ice,\max}$ (kg m^{-2}) are the snowfall rate and the maximum canopy load for snow, respectively:

$$M_{ice,\max} = \alpha(0.27 + 46/\rho_s)LSAI, \tag{12}$$

where the fresh snow density, $\rho_s = 67.92 + 51.25e^{(T_{air}-273.16)/2.59}$ (kg m^{-3}), and T_{air} is the air temperature at reference height. *Schmidt and Gluns* [1991] made extensive measurements that suggest $\alpha = 6.6$ and 5.9 kg m^{-2} for pine and spruce, respectively. In contrast to the maximum load for liquid water, $M_{liq,\max} = 0.1LSAI$ (kg m^{-2}), $M_{ice,\max}$ is

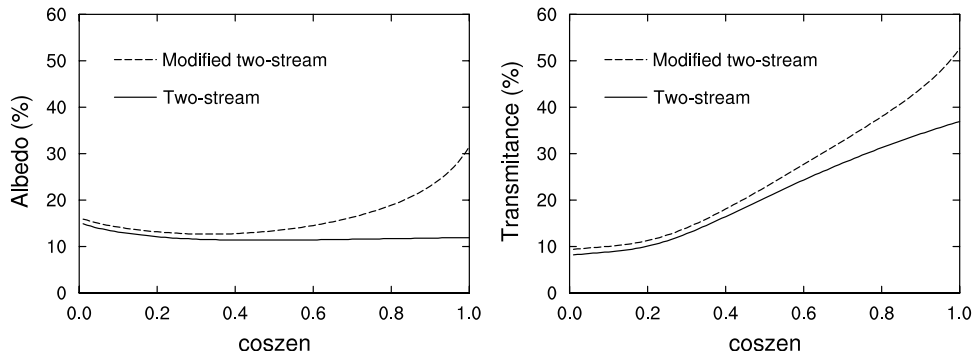

Figure 3. Surface albedo and canopy transmittance as a function of the cosine of the solar zenith angle calculated from the two-stream radiation-transfer scheme and the modified two-stream radiation-transfer scheme for a needleleaf evergreen tree with the NCAR LSM1.0 default parameters and LSAI = 2.

about 48 times greater than $M_{liq,\max}$ for pine when ρ_s = 100 kg m^{-3}.

[15] *Roesch et al.* [2001] parameterized the unloading rate of snow from the canopy, R_{unload}, as a function of wind speed at a reference height, v, and canopy temperature, T_c:

$$R_{unload} = M_{ice}[f(T_c) + f(v)], \quad (13)$$

where $f(T_c) = (T_c - 270.15)/C_T$, and $f(v) = v/C_v$. $C_T = 1.87 \times 10^5$ to allow for the unloading of half the intercepted snow during 12 hours at $T_c = 0°C$, and $C_v = 1.56 \times 10^5$ to allow for the unloading of half the intercepted snow within 6 hours when $v = 5$ m s^{-1}.

[16] Melting occurs only when ice exists ($M_{ice} > 0$) on the canopy and the canopy temperature is above the freezing point ($T_c > T_{frz}$); refreezing occurs only when liquid water exists ($M_{liq} > 0$) and the canopy temperature is below the freezing point ($T_c < T_{frz}$). The melting rate, R_{melt}, and the refreezing rate, R_{frz}, are parameterized as follows:

$$R_{melt} = \min\left[M_{ice}/\Delta t, C_{ice}(M_{ice}/\rho_{ice})\left(T_c - T_{frz}\right)/(L_{il}\Delta t)\right], \quad (14)$$

$$R_{frz} = \min\left[M_{liq}/\Delta t, C_{liq}\left(M_{liq}/\rho_{liq}\right)\left(T_{frz} - T_c\right)/(L_{il}\Delta t)\right], \quad (15)$$

where $C_{ice} = 2.094 \times 10^6$ (J m^{-3} K^{-1}) and $C_{liq} = 4.188 \times 10^6$ (J m^{-3} K^{-1}) are the volumetric heat capacity of ice and liquid water. ρ_{ice} and ρ_{liq} are the densities of ice (917 kg m^{-3}) and liquid water (1000 kg m^{-3}). L_{il} is the latent heat of fusion (=0.3336 $\times 10^6$ J kg^{-1}). As a result of melting and refreezing, the canopy temperature, T_c', is updated as a weighted average of the temperatures of the snow-covered fraction, f_{sno}, and the snow-free fraction, $(1 - f_{sno})$:

$$T_c' = f_{sno}T_{frz} + (1 - f_{sno})T_c, \quad (16)$$

where $f_{sno} = \left(\frac{M_{ice}}{M_{ice,\max}}\right)^{2/3}$, following *Deardorff* [1978].

[17] The energy-balance equation of the canopy in VISA is modified to include the canopy heat capacity, which is parameterized as a function of LSAI, and the canopy ice storage, M_{ice}, and liquid water storage, M_{liq}:

$$C_c = 0.02LSAIC_{liq} + C_{ice}(M_{ice}/\rho_{ice}) + C_{liq}\left(M_{liq}/\rho_{liq}\right). \quad (17)$$

The effects from this modification on the surface temperature will be discussed later.

2.3. Under-Canopy Sensible Heat Flux

[18] The aerodynamic resistance to sensible heat flux for bare snow or bare soil and that for the above-canopy sublayer were derived from Monin-Obukhov similarity theory with stability corrections [*Bonan*, 1996]. The aerodynamic resistance to sensible heat flux for the under-canopy sublayer, r_{ah}, was derived from *Choudury and Monteith* [1988]:

$$r_{ah} = \int_{z_{0g}}^{d+z_{0v}} dz/K_h(z), \quad (18)$$

where d, z_{0v}, and z_{0g} are the zero displacement height, the canopy roughness length, and the ground roughness length, respectively. In uniform vegetation, it is assumed that the eddy diffusivity, $K_h(z)$, has an exponential profile within the canopy:

$$K_h(z) = K_h\left(H_{top}\right)e^{-a\left(1-z/H_{top}\right)}, \quad (19)$$

where a is the absorption coefficient of momentum, and $K_h(H_{top}) = \kappa u_*(H_{top} - d)$ is the eddy diffusivity (m^2 s^{-1}) for heat at the top of the canopy, where κ is the von Karman constant. Substituting equation (19) into equation (18) gives:

$$r_{ah} = \frac{H_{top}}{aK_h\left(H_{top}\right)}\left[e^{a\left(1-z_{0g}/H_{top}\right)} - e^{a\left(1-(z_{0v}+d)/H_{top}\right)}\right]. \quad (20)$$

Brutsaert [1982] provided a thorough discussion on the absorption coefficient of momentum, which varies widely from 2.2 for wheat to 4.25 for pine forest. The general value (a = 3) was used as the default value in VISA independent of vegetation types. *Goudriaan* [1977] derived a from the momentum transfer equation as a function of the canopy density (LSAI), canopy height (H_{top}), vegetation type, and the stability correction factor (Φ_m):

$$a = \left(c_d H_{top} LSAI/l_m\right)^{0.5}(\Phi_m)^{0.5}, \quad (21)$$

where c_d is the drag coefficient of leaves and l_m is the mean mixing length, which is the free space between the leaves and stems depending on vegetation types. For a coniferous tree, $c_d = 0.2$ and $l_m = 1.13$ m [*Goudriaan*, 1977]. Φ_m is the stability correction factor for momentum. According to *Businger et al.* [1971]:

$$\begin{array}{llll} \Phi_m = (1 - 15z/L)^{-0.25} & \text{unstable} & z/L < 0 \\ \Phi_m = 1.0 + 4.7z/L & \text{stable} & z/L > 0 \end{array}, \quad (22)$$

where $z = d + z_{0v}$ and L is the Monin-Obukhov length below the canopy:

$$L = \frac{u_*^3}{\kappa(g/T_a)\left(H_g/(\rho_a C_P)\right)}, \quad (23)$$

where g is the gravitational acceleration, ρ_a is the air density, C_P is the specific heat of air at constant pressure, u_* is the friction velocity, T_a is the air temperature within the canopy, and H_g is the sensible heat flux from the ground (z_{0g}) to the canopy air ($d + z_{0v}$). When the LSAI equals 2.0, a varies from 2 under a neutral condition to about 6 under a stable condition (Figure 4).

3. BOREAS Data and Experiment Design

[19] The BOREAS study region covered most of Saskatchewan and Manitoba, containing northern study areas (NSA) and southern study areas (SSA) within which process study sites were located [*Sellers et al.*, 1997]. A more detailed description of the site locations, site environments, and instrumentation can be found in the work of *Shewchuk* [1997]. We chose to use data obtained from the

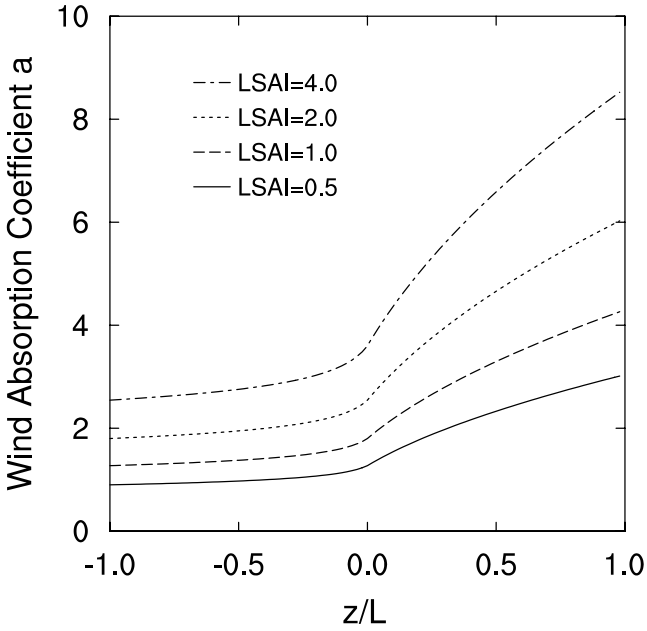

Figure 4. The absorption coefficient of momentum, a, as a function of z/L for different LSAI values.

SSA-OJP (53.9°N, 104.7°W, and elevation = 579 m). The continuous above-canopy meteorological data for the site, which were obtained from automatic meteorological stations, were used as upper boundary conditions to force VISA. Measurements of surface albedo, snow depth, surface radiative temperature, and under-canopy solar radiation were used to validate and test the model.

[20] We represented the old jack pine at SSA-OJP by one plant functional type (needleleaf evergreen tree) in the model grid-cell instead of the mosaic surface type 3 in the work of *Bonan* [1996, Table 5], which is composed of two plant functional types: 75% needleleaf evergreen tree and 25% bare soil. The vegetation physiological parameters (e.g., leaf and stem reflectance, leaf and stem transmittance, leaf orientation, and photosynthetic properties) and soil parameters were assigned to values following *Bonan* [1996] and *Bonan et al.* [1997]. The canopy geometry parameters follow *Yang and Friedl* [2003] and are given in Table 1. Table 2 lists a series of experiments that were conducted to investigate the impacts of the modified formulation in section 2 on snow energy and mass balances. The control run (CTRL) used the same parameters as in the NCAR LSM1.0. We conducted one experiment (ADJ-LAI) to investigate how the adjustment of LSAI from the default value (4.7) in CTRL to the observed value (1.89) impacts canopy radiation transfer and surface albedo. We then conducted experiments to examine the effects from using the modified two-stream radiation transfer scheme (MOD-RAD), the snow-interception model (SNO-INT), the inclusion of the canopy (including canopy intercepted snow) heat capacity into the canopy energy balance equation (HEAT-CAP), and the stability correction to a (STA-COR). We also conducted four sensitivity experiments to investigate how snowmelt responds to various values of a. The snow submodel and its parameters were kept unchanged in all the experiments.

4. Results

4.1. Under-Canopy Solar Radiation

[21] We compared the model-simulated under-canopy solar radiation fluxes from CTRL, ADJ-LAI, and MOD-RAD to the data taken from the SSA-OJP site between 7 and 11 February 1994 (Figure 5). The default LSAI value, which was prescribed for needleleaf evergreen tree in the NCAR LSM1.0, is too high to reproduce the observed under-canopy solar radiation flux. In CTRL, LSAI is 4.7 in February, which results in a simulated flux of the under-canopy solar-radiation that is considerably lower than the observed. Adjusting the LSAI to the observed value of 1.89 significantly increases the simulated under-canopy solar radiation flux to agree with observations. For example, the daily mean net short-wave radiation flux at the snow surface increases from 0.78 to 8.27 Wm^{-2} on 2 March 1994 (day 61) (Table 3). The net long-wave radiation decreases from 10.39 to 1.29 Wm^{-2} because of the decrease in canopy-emitted long-wave radiation. The modified two-stream radiation transfer scheme (MOD-RAD) produces fluxes that more closely resemble the observed fluxes. However, the influences of introducing the gap probabilities are minor because the cosine of the solar zenith angle at noon, the maximum value during a day between 7 and 11 February, is only about 0.23.

[22] The leaf orientation (χ_L) affects under-canopy solar radiation flux: vertical leaves transmit more light than other orientations do. Also, such transmittance depends on the solar zenith angle. In the case of $\mu = 1.0$ and LSAI = 1.89, the transmittance of solar radiation through a needleleaf tree increases from 0.389 for randomly oriented leaves (χ_L = 0.01) to 0.494 for vertical leaves ($\chi_L = -0.4$), which is an increase by 27%. However, when $\mu = 0.23$ and LSAI = 1.89, the transmittance increases only by 6% (from 0.117 to 0.124).

4.2. Surface Albedo

[23] Figure 6 shows a time series of the modeled and observed daily mean surface albedo at SSA-OJP. The

Table 2. List of Experiments

Experiments	Description
CTRL	the default model, as in the NCAR LSM 1.0 [*Bonan*, 1996]
ADJ-LAI	as in CTRL, but LSAI is adjusted from 4.7 to 1.89
MOD-RAD	as in ADJ-LAI, but with the modified two-stream radiation transfer as described in section 2.1
SNO-INT	as in MOD-RAD, but with the snow-interception model as described in section 2.2
HEAT-CAP	as in SNO-INT, but with the inclusion of the canopy heat capacity as described in equation (17) into the canopy energy-balance equation
STA-COR	as in HEAT-CAP, but with the stability correction to a as described in section 2.3
Sensitivity tests	sensitivity tests of various absorption coefficients of momentum based on STA-COR, but excluding the stability correction to a

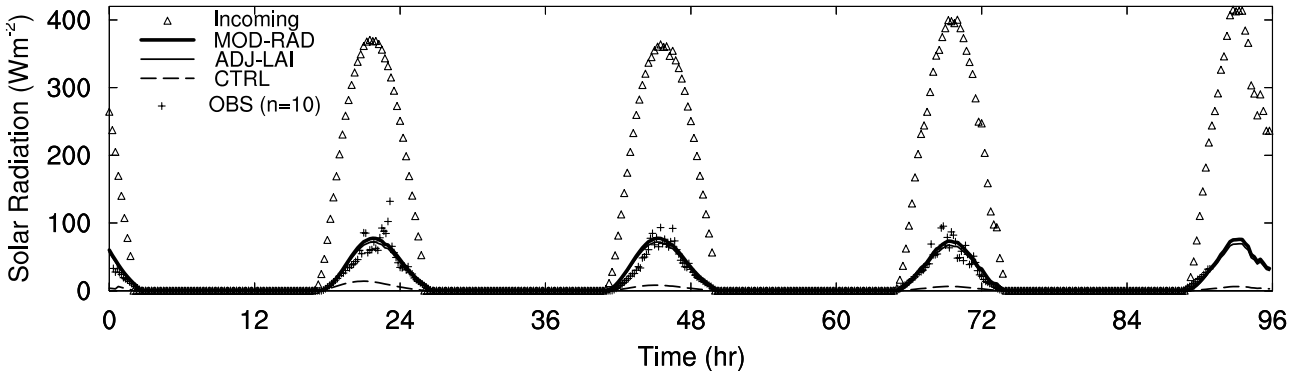

Figure 5. Comparison of modeled and observed under-canopy solar radiation fluxes at the SSA-OJP site, taken during 7–11 February 1994. The observed incoming (above canopy) solar radiation fluxes (triangles) are also included for reference.

observed surface albedo was derived from the in situ observed incoming and reflected solar radiation at the forest site. Spurious values of the derived surface albedo occurred when the recorded daily mean incoming solar radiation was below 20 Wm^{-2}. This low value was presumably caused by snow or ice on the upward looking radiometer [*Betts and Ball*, 1997]. These occurrences are represented by circles on the abscissas in Figure 6.

[24] The simulated daily mean albedo at SSA-OJP from the CTRL run is higher in midwinter and lower in spring than the observed daily mean albedo (Figure 6a). After the LSAI was adjusted from the default value (4.7) to the observed value (1.89), the simulated albedo for the spring season closely resembles the observed albedo for this period, but the simulated albedo for the midwinter season does not approximate the observed albedo (Figure 6b). The decreased LSAI makes the vegetation canopy more transparent, which allows more solar radiation to be transmitted downward and upward through the canopy. The treatment of canopy snow interception in the same fashion as canopy rain interception in the default VISA causes the fractional snow cover on the canopy to be overestimated. This results in overestimated surface albedos in wintertime (for instance, see the simulated albedos in the CTRL run (Figure 6a) and MOD-RAD (Figure 6b) for the period between day 300 and day 360). The SNO-INT run dramatically decreases the overestimated albedos from 0.35 to about 0.2 by lowering the fractional snow cover on the canopy (Figure 6c). When the snow-interception model is applied, the amount of snow intercepted by the canopy is increased by a factor of 10 (SNO-INT in Figure 7a), because the maximum interception capacity for snow (equation (12)) is about 50 times greater than that for rain. However, the intercepted snow often does not remain on the vegetation canopy for long periods of time because of the unloading caused by wind and temperature. The wet fraction (the canopy fractional snow cover in winter) is largely decreased (Figure 7b) because of the snow unloading mechanisms and the larger maximum interception capacity for snow. The canopy-intercepted snow and the fractional snow cover on the canopy are considerably sensitive to the parameters of α in equation (12) and C_v in equation (13).

[25] The diurnal variations of surface albedo for different phases are shown in Figure 8. The two-stream parameterization essentially reproduces the diurnal variations of observed surface albedo, especially for periods when there is no snow on the canopy or on the ground (Figure 8c). The CTRL run overestimates surface albedo in the snow-falling phase and underestimates albedo in the snow-melting phase. These discrepancies are eliminated by introducing the snow-interception model (the SNO-INT run) in the snow-falling phase and by reducing LSAI (the MOD-RAD run) in the snow-melting phase. The two-stream radiation transfer scheme modified to include the canopy gap probabilities shows the effects on the simulation of the surface albedo in the snow-melting phase when the cosine of the solar zenith angle is increasing (Figure 8b). Both the observed and the simulated surface albedos from the MOD-RAD run and the SNOW-INT run show "W" shapes in the snow-melting phase, most noticeable on days of 451, 455, 457 and 458 (Figure 8b). In contrast to the "U" shape surface albedos in the summer season (Figure 8c), these "W"-shape surface albedos (Figure 8b) result from the underlying snow surface and the diurnal variations of the gap probabilities, whose parameterizations are included in both MOD-RAD and SNOW-INT. As a function of the solar zenith angle, the gap probability reaches its maximum value at noon resulting in a peak surface albedo when the underlying snow surface is mostly exposed.

4.3. Sensitivity of Snowmelt to the Canopy Absorption Coefficient of Momentum

[26] *Choudury and Monteith* [1988] tested the sensitivity of the soil-surface temperature to the canopy absorption

Table 3. Daily Mean Energy Budgets on the Snow Surface on 2 March 1994[a]

Experiments	a	$T_{rad,\max}$	SW_{net}	LW_{net}	LE	SH	SM
CTRL	3	287.11	**0.78**	**10.39**	4.96	−40.89	55.19
ADJ-LAI	3	285.84	**8.27**	**1.29**	4.82	−42.57	57.99
MOD-RAD	3	**285.76**	9.00	1.16	4.79	**−42.01**	**58.05**
SNO-INT	3	**284.89**	9.05	0.62	1.79	**−38.85**	**57.51**
HEAT-CAP	3	**282.34**	9.10	0.32	1.71	**−18.89**	**34.69**
STA-COR	3.62	**283.13**	9.10	1.99	2.45	**−11.97**	**28.53**

[a]Day 61 in Figure 11. Boldface values represent significant changes from one experiment to another. $T_{rad,\max}$ is the daily maximum value of the surface radiative temperature in K; SW_{net} and LW_{net} are the net shortwave and longwave radiation fluxes in Wm^{-2} (positive downward); LE and SH are the latent heat and sensible heat fluxes in Wm^{-2} (positive upward); SM is the energy available for melting snow in Wm^{-2}.

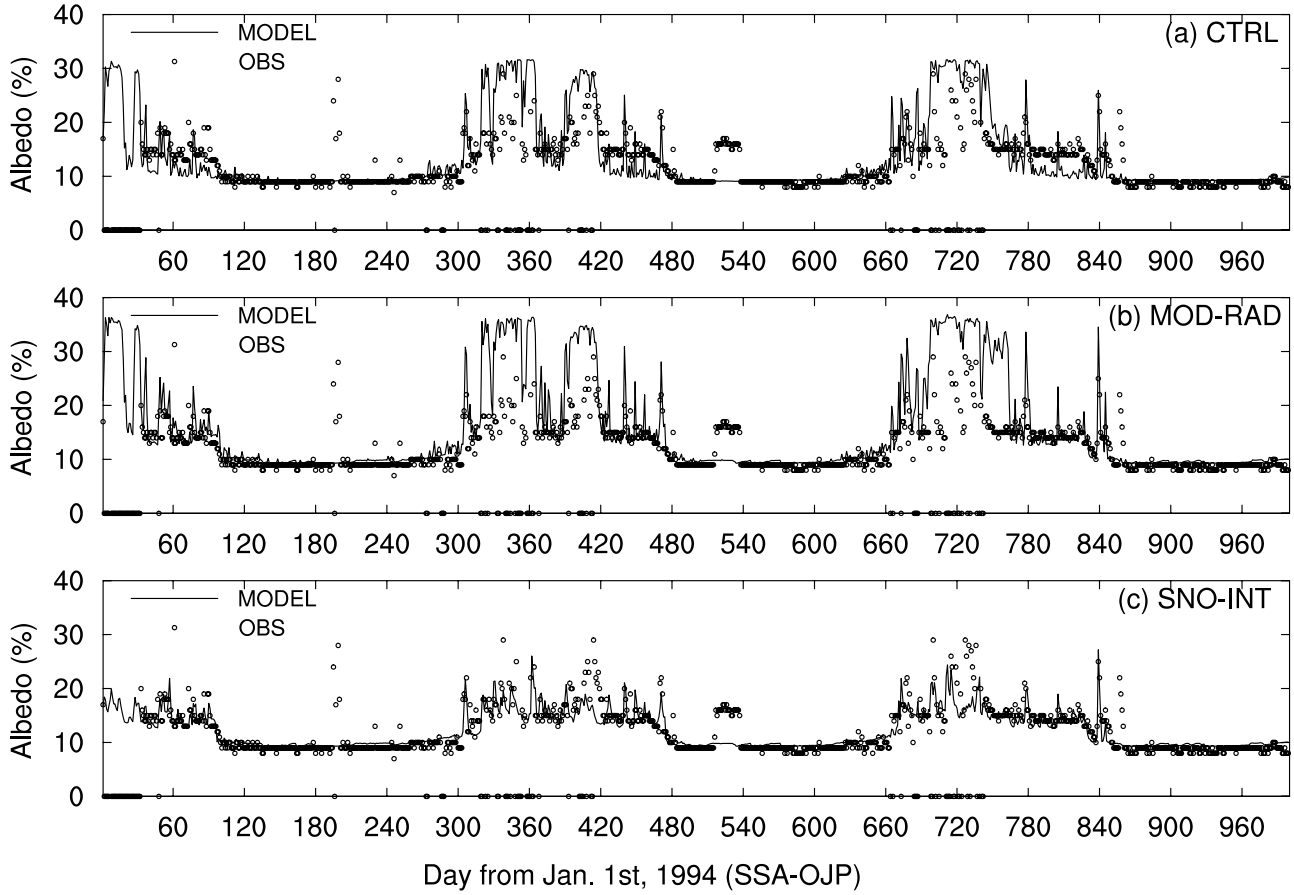

Figure 6. Comparison of modeled and observed daily mean surface albedos: (a) CTRL, (b) MOD-RAD, and (c) SNO-INT for a period of 1994–1996 at SSA-OJP.

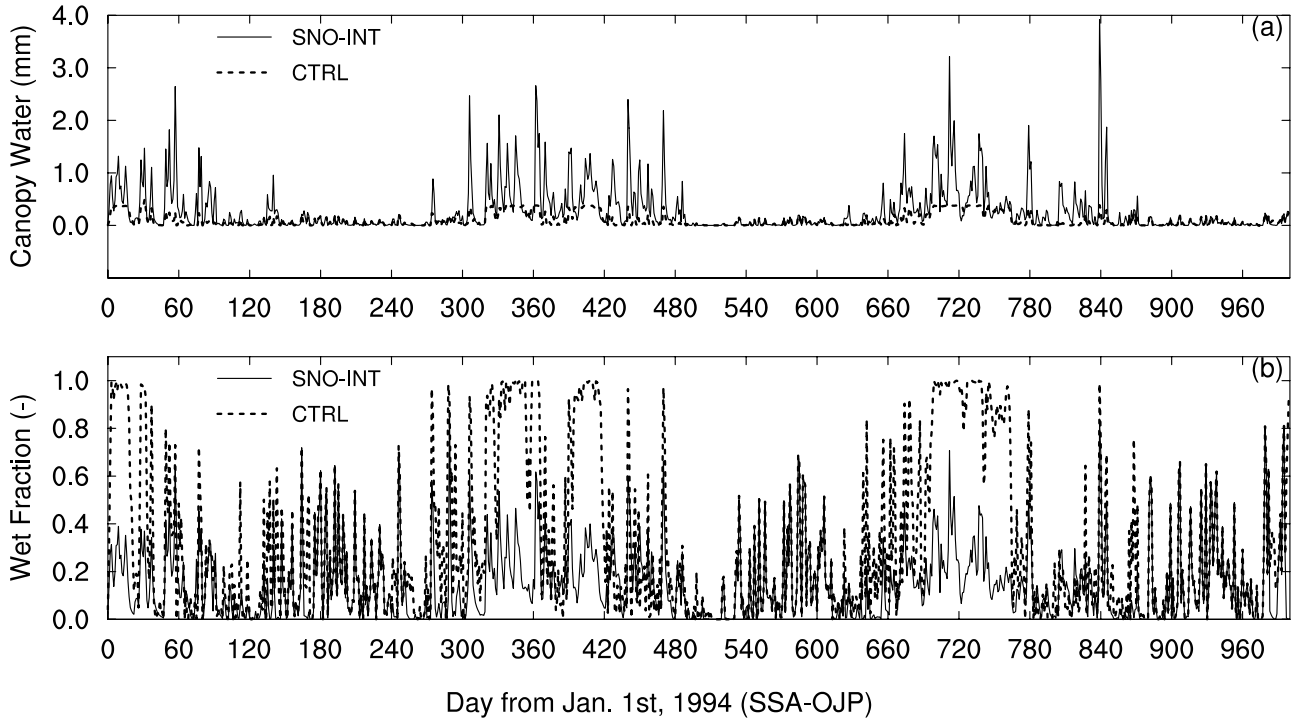

Figure 7. The modeled (a) canopy water storage and (b) wet fraction (or canopy snow fraction in winter) from CTRL and the SNO-INT.

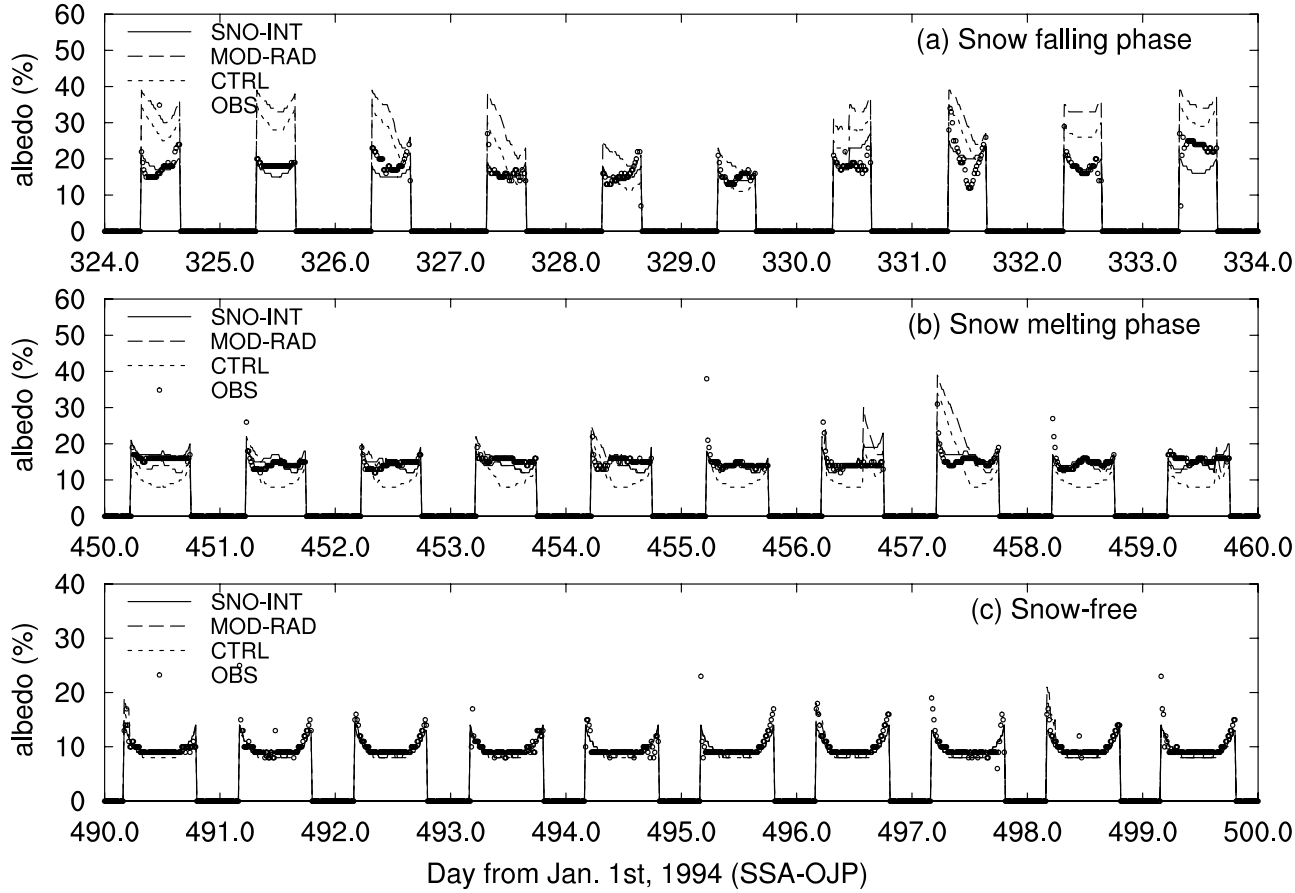

Figure 8. Modeled diurnal variations of surface albedos from various experiments at SSA-OJP for (a) the snow-falling phase, (b) the snow-melting phase, and (c) the snow-free period.

coefficient of momentum, a. Their results showed that the soil surface temperature at noon increases by five degrees when a varies from 2.0 to 3.0. In contrast to the soil-surface temperature, the snow surface temperature remains at the freezing point when snowmelt occurs at noon, but the energy available for melting snow decreases. Figure 9 shows how a affects snow ablation. Because snowmelt often occurs only around noon on the warmer days in spring or early summer, the analysis of the diurnal cycle of energy balances at the snow surface can clearly reveal the influences of the vegetation canopy on snow ablation. Figure 9a shows the diurnal cycle of the sensible heat flux from the snow surface. Figure 9b shows the diurnal cycle of the energy available for melting snow. The daily mean snow depth for the years 1994 and 1995 is shown in Figure 9c. For example, on day 61, as a increases from 2.0 to 5.0, the sensible heat flux from the canopy downward to the snow surface decreases from around 100 Wm^{-2} to less than 30 Wm^{-2} as a result of the decreased turbulent motions. The snow-melting energy correspondingly decreases from 150 Wm^{-2} to 70 Wm^{-2}. The modeled snow depth increases to fit the observed with $a = 5$ producing the most realistic result.

4.4. Effects of Canopy Heat Capacity on Surface Temperature and Snowmelt

[27] Figure 10 shows the ways in which the simulated net radiation and surface radiative temperature differ between the CTRL run and the STA-COR run. Although the net radiation at the surface is almost the same in both runs (Figure 10a), the surface radiative temperature from the STA-COR run decreases during the day and increases significantly during the night to match the observed (Figure 10b). This improvement can be mainly attributed to the buffer effects from the inclusion of the canopy heat capacity (equation 17) into the canopy energy-balance equation, and partly attributed to the heat release and consumption associated with freezing and melting, which is parameterized as in equation (16). The daily maximum value of the surface temperature on 2 March 1994 simulated by SNO-INT is 0.87 K lower than that simulated by MOD-RAD (Table 3); this difference is associated with the phase change of the canopy water. However, it is decreased by 2.45 K (comparing SNO-INT with HEAT-CAP) (Table 3) due to the inclusion of the canopy heat capacity (equation 17) into the canopy energy-balance equation. The daily mean downward sensible-heat flux is decreased from 38.85 Wm^{-2} (SNO-INT) to 18.89 Wm^{-2} (HEAT-CAP). Consequently, the energy available for melting snow is decreased by 22.82 Wm^{-2}. Note that the second and the third terms on the right hand of equation (17) are much less than the first term unless in the event of extremely great snowfall. Compared to the advective energy carried by rainfall to the snow surface, the advective energy carried by the

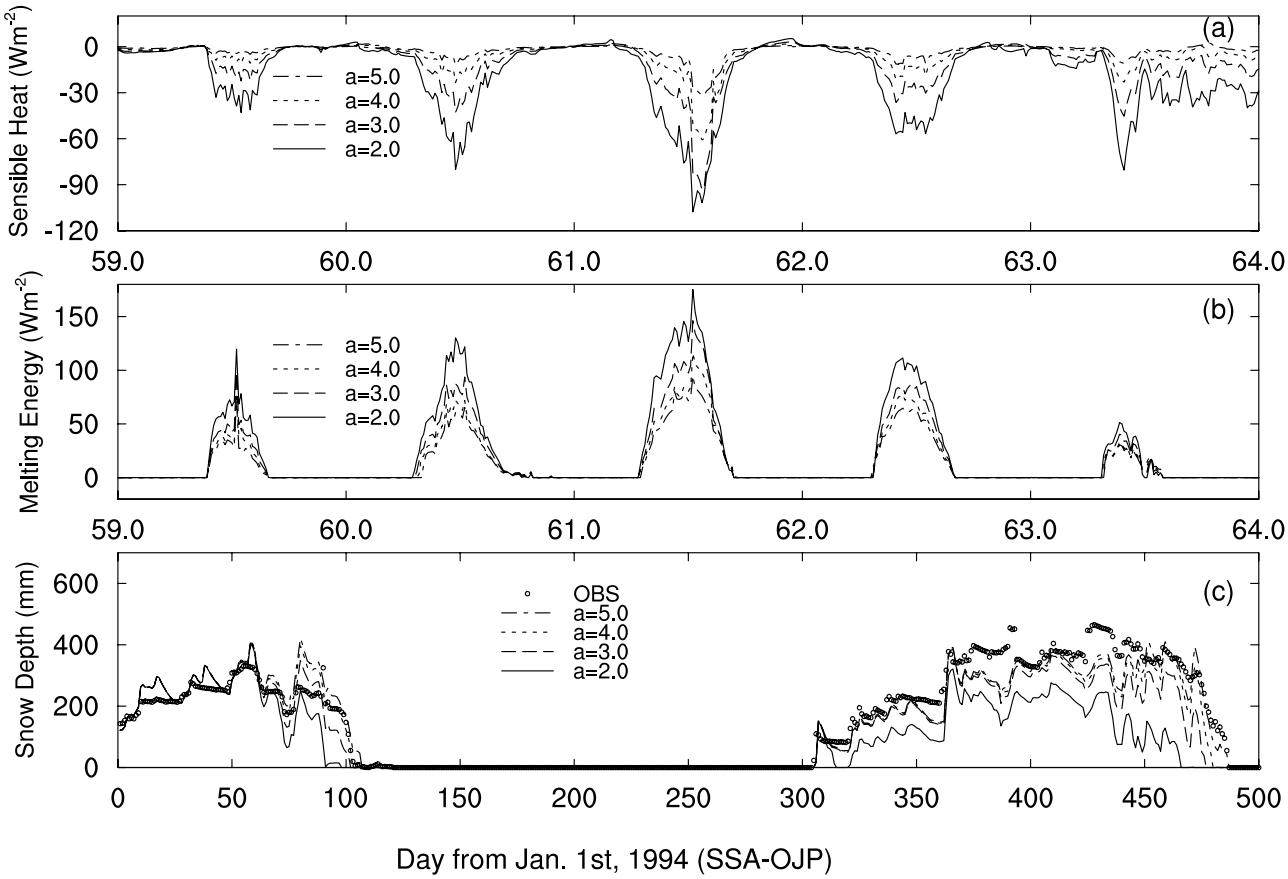

Figure 9. Sensitivity to various canopy absorption coefficients of momentum for (a) the sensible heat flux between the canopy and the snow surface (positive upward), (b) the energy available for melting snow, and (c) the daily mean snow depth. Observations are also included in Figure 9c.

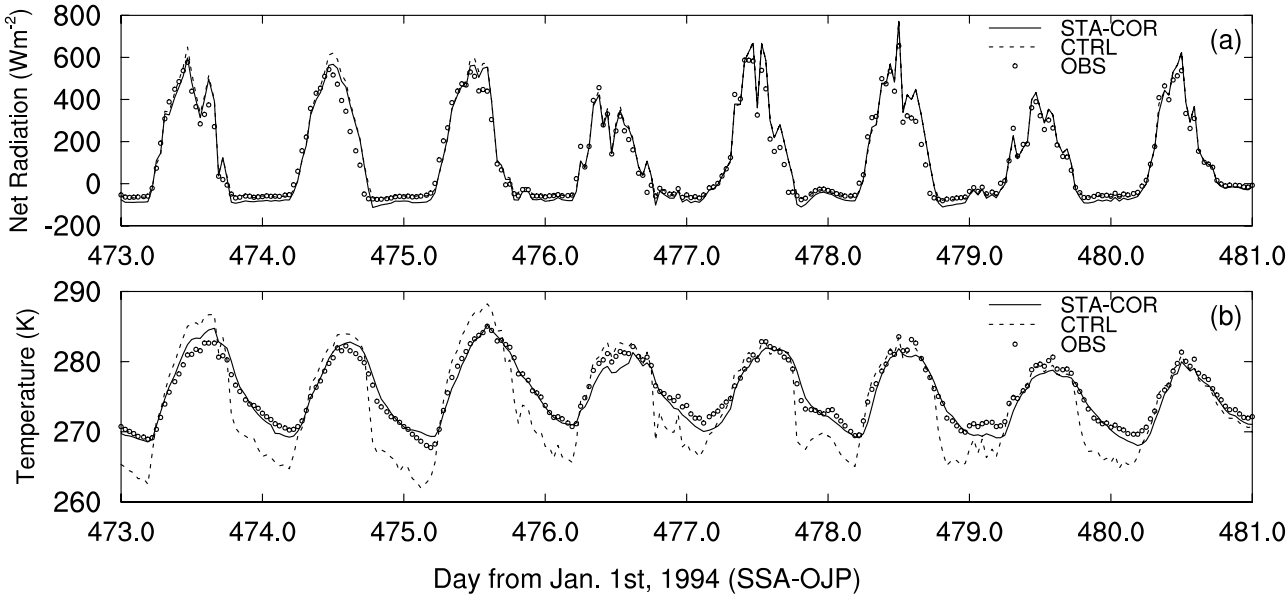

Figure 10. Modeled diurnal variations of (a) net radiation and (b) surface radiative temperature in comparison with observations.

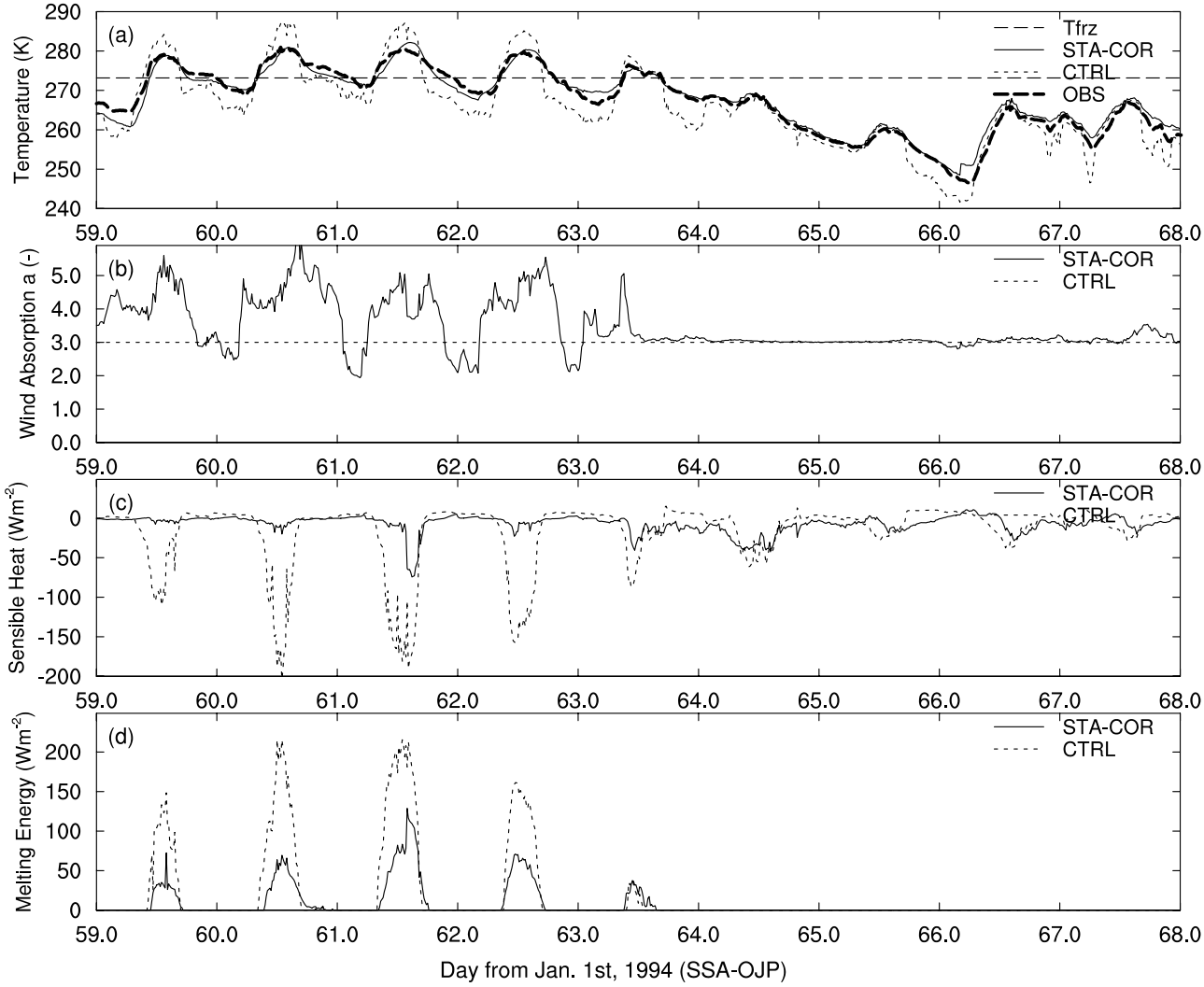

Figure 11. Modeled (a) surface radiative temperature, (b) canopy absorption coefficient of momentum, (c) sensible heat flux between the canopy and the snow surface (positive upward), and (d) energy for melting snow. Observations are also included in Figure 11a.

unloaded snow from the canopy was considered negligible in this study.

4.5. Effects of Stability Correction to the Canopy Absorption Coefficient of Momentum and Snowmelt

[28] In the STA-COR run, a remains approximately 4.5 during the day when a warm vegetation canopy overlies the cold snow on the ground creating a strong stable condition (Figure 11b). The downward sensible heat flux between the vegetation canopy and the snow surface greatly decreases from 150 Wm^{-2} to 20 Wm^{-2} (positive upward) around noon (Figure 11c), and the energy available for melting snow decreases from 200 to 100 Wm^{-2} (Figure 11d). This reduction of the available energy for melting snow can mainly be attributed to the inclusion of the canopy heat capacity term (equation 17) in the canopy energy-balance equation and the stability correction to a. Including only the stability correction to a results in a reduction of the daily mean downward sensible heat flux by 6.92 Wm^{-2} (Table 3). Correspondingly, the daily mean available energy for melting snow is reduced by 6.16 Wm^{-2}.

5. Discussion

5.1. Implications of Site-Specific LAI for Boreal Forests in General

[29] The ADJ-LAI experiment demonstrates that reducing LAI to match the in situ measurement at the BOREAS SSA-OJP site improves the simulation of surface albedo and the under-canopy solar radiation flux. It is possible that the original LAI value of 4.2 is too high for needleleaf evergreen trees in general. We addressed this possibility in Table 4, where the February LAI used in VISA and NCAR LSM1.0 is compared with satellite data-derived LAI for needleleaf evergreen trees in a large North American region (40–60°N, 60–130°W) (Table 4). Care was taken to convert the LAI used in the models, defined with respect to vegetated area only, to values per unit ground area in the region, consistent with the satellite products. The converted regional LAI in

Table 4. Comparison of February Leaf Area Index and Stem Area Index for Needleleaf Evergreen Trees Used in Models and Derived From Satellite Data[a]

		Regional Averaged (40–60°N, 60–130°W)		
Data Sources	Reference	LAI	SAI	LSAI
NCAR LSM1.0	*Bonan* [1996]	2.32	0.28	2.60
VISA	this study			1.05[b]
CLM2.0	*Bonan et al.* [2002]	0.82	0.16	0.98
Common land model	*Zeng et al.* [2002][c]	1.50	0.75	2.25
AVHRR	*Myneni et al.* [1997][d]	0.73		>0.73
MODIS	*Tian et al.* [2004][c]	0.42		>0.42

[a]LAI, leaf area index; SAI, stem area index.
[b]The value is derived by the following approach. In NCAR LSM1.0, scaling from LSAI with respect to the ground area covered by needleleaf evergreen trees only (4.7) to LSAI with respect to the North American region (2.6) gives a ratio of 2.6/4.7. Applying the same ratio to VISA led us to have LSAI = 1.89 × (2.6/4.7) = 1.05.
[c]The values for the common land model and MODIS are from *Tian et al.* [2004, Figure 10].
[d]The 1982–2000 averaged AVHRR monthly 1° × 1°.

NCAR LSM1.0 is 2.32, higher than satellite estimates (0.73 by AVHRR and 0.42 by MODIS). Although the MODIS estimate may be too low in the presence of snow [*Tian et al.*, 2004], the value in NCAR LSM1.0 is likely too high. As a comparison, *Bonan et al.* [2002] and *Zeng et al.* [2002] reported values of 0.82 and 1.50, respectively, for the Community Land Model version 2.0 (CLM2.0) and the Common Land Model (CLM). The in situ LSAI value of 1.89 for needleleaf evergreen trees adopted in this study would be equivalent to a value of 1.05 for the North American Region for boreal forests, compared well with 0.98 in CLM2.0 [*Bonan et al.*, 2002]. The LSAI value used in the Common Land Model [*Zeng et al.*, 2002] is about twice that of VISA. Because of its high LSAI, the Common Land Model underestimated the wintertime surface visible albedo in boreal forest regions [*Zhou et al.*, 2003].

[30] The agreement of the simulated under-canopy solar radiation flux and the surface albedo with those observed in SSA-OJP also indicates that the prescribed vegetation physiological parameters (e.g., leaf and stem reflectance, leaf and stem transmittance, and snow optical properties) for needleleaf evergreen trees are sufficiently accurate when there are no observational data available. If there are only small-scale gaps in the boreal forest, the bare soil fraction in a "mosaic" land model is conceptually comparable to the between-crown gap possibility, P_{bc}. However, the bare soil fraction in a "mosaic" land model is fixed without diurnal variations, and the within-crown gap possibility, P_{wc}, is entirely neglected in a "mosaic" land model. The fractional tree cover derived from the remote-sensing products corresponds to $1 - P_{bc}$ for the sun angle of observation.

5.2. Application of the Schemes in a Different Site

[31] To evaluate the capability of the newly introduced schemes to simulate snow mass on the canopy and on the ground in an environment different from BOREAS, we conducted several experiments using the meteorological and hydrological data gathered by *Storck et al.* [2002] in the Umpqua National Forest, Oregon (42.9°N, 122.1°W, and elevation = 1200 m). We first calibrated the snow/rain criterion to reproduce the observed snow water equivalent (SWE) measured in the clearing (shelterwood). The closest agreement between the modeled and the observed SWE is obtained when the snow/rain criterion equals to 0.4°C (Figure 12b) and the snow surface roughness is assumed to be 0.005 m. The modeled canopy-intercepted SWE

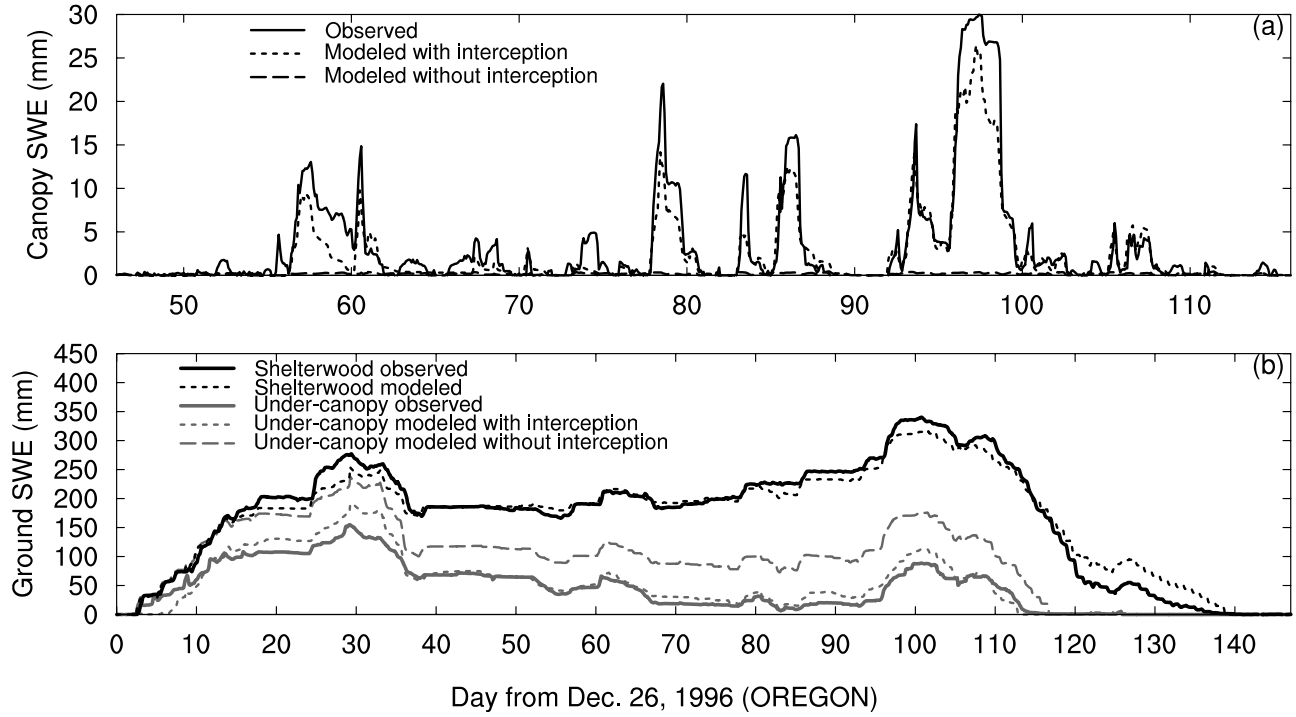

Figure 12. Comparison of simulated and observed snow water equivalent (SWE) (a) on the canopy and (b) on the ground in a clearing (shelterwood) and beneath a Douglas fir in Oregon.

agrees well with the observed (Figure 12a) when $M_{ice,\max}$ = 40 kg m^{-2}, an extremely large value, which was suggested by *Storck et al.* [2002], and $C_v = 3.5 \times 10^5$ m. At this site, snow removal from the canopy is dominated by sloughing which in turn is controlled by temperature, rather than wind. Excluding the temperature factor, $f(T_c)$ in equation (13), failed to reproduce the observed canopy-intercepted snow during the snow-unloading period. The model also reproduces the under-canopy SWE with the observed H_{top} (11.0 m) and the derived z_{0v} (0.65 m) and d_0 (7.35 m) from H_{top}. A sensitivity experiment without the snow interception model overestimates the under-canopy SWE by 60–70 kgm^{-2} during most of the snowing season. Evaluation on the sublimation scheme of the canopy-intercepted snow in VISA will be addressed in future studies.

5.3. Further Remarks on the Under-Canopy Turbulence

[32] It should be pointed out that a more elaborate determination of a for a forest environment is complicated because of the variable values of the mixing length scale (l_m) within and under the forest canopy. The variable l_m in equation (21) can be understood as a mean mixing length for the different canopy sublayers. To be consistent with the radiation transfer, an equation for a should include more canopy geometric parameters. l_m in equation (21) should be expressed as a combination of the mixing lengths for the canopy roughness sublayer, the within-canopy layer, and the under-canopy layer. In the under-canopy layer, air flow is broken down into smaller eddies by tree trunks at a scale of d_r/0.21, where d_r is the diameter of a trunk [*Poggi et al.*, 2004] with an upper limit of the free space under the canopy, which is estimated as $(H_{bot}/\rho_t)^{1/3}$ (about 2.47 m for the SSA-OJP case). In the canopy roughness sublayer, l_m should be a superposition of that of the classical boundary layer at a scale of $(z - d)$ and that of the wake vortices at a scale comparable to individual drag elements. In the within-canopy sublayer, l_m is limited by the free space between leaves and stems. However, a development of a sound parameterization of a for use in GCMs requires more wind and temperature profile data than currently available.

6. Conclusion

[33] In this paper, a series of experiments were conducted to evaluate the newly introduced parameterization schemes of radiation transfer through the vegetation canopy, the interception of snow by the vegetation canopy, and the under-canopy turbulent sensible heat transfer. The VISA model was validated against the BOREAS SSA-OJP and Oregon data sets.

[34] When LSAI is reduced from the default value (4.7) to match the observed value (1.89), the two-stream radiation-transfer scheme used in the default VISA accurately simulates the transferring of solar radiation through the vegetation canopy. The 3-D canopy geometry, parameterized as gap probabilities, has favorable but minor influences on the modeled radiation flux received by the snow surface in midwinter because of the large solar zenith angle in high-latitude regions. Taking into consideration the 3-D canopy geometry may have greater influence on modeling the solar radiation transfer and the surface albedo in the late spring season, when the solar zenith angle increases; the simulated surface albedos show "W" shapes.

[35] Parameterization of canopy-intercepted water can affect the wintertime surface albedo during snowfall phases. By lowering the fractional snow cover on the canopy, the snow-interception model, which explicitly describes the loading and unloading of snow and the melting and refreezing of snow, can reduce the overestimated surface albedo produced by the default model. Although the amount of canopy-intercepted water in the snow interception model is greater by a factor of 10 than in the default model, the fractional snow cover on the canopy in the snow-interception model is much lower than that in the default model due to the unloading mechanisms and the larger maximum interception capacity for snow than that for rain. The canopy-intercepted snow and the fractional snow cover on the canopy are very sensitive to the maximum loading capacity of snow and the estimated unloading factors of wind and temperature.

[36] When the heat capacity of the canopy and canopy-intercepted water is incorporated in the canopy energy balance equation, the surface radiative temperature decreases during the day and increases significantly at night closely resembling observations. This improvement is mainly due to the buffer effects that result from the added canopy heat storage term and due in part to the heat released when water refreezes during the night and the heat consumed when snow melts during the day. The improvement in simulating the surface radiative temperature greatly contributes to the reduction of the modeled excessive sensible heat fluxes during the day. The canopy absorption coefficient of momentum strongly affects the turbulent sensible heat flux below the vegetation canopy. During snow-melting season, the warm canopy overlying cold snow on the ground may form a strongly stable condition, which significantly suppresses turbulence transfer and results in a larger absorption coefficient of momentum. Thus the stability correction to the canopy absorption coefficient of momentum can considerably reduce the excessive downward turbulent sensible heat flux from the vegetation canopy to the snow surface. However, a more elaborate determination of the canopy absorption coefficient of momentum requires more observed profiles of wind and temperature under, within, and above the vegetation canopies than currently available.

[37] **Acknowledgments.** This work was funded by NASA grant NAG5-12577 and NAG5-10209. The authors would like to thank Dennis Lettenmaier and Pascal Stork for providing us the Oregon Data set. Robert E. Dickinson is thanked for his invaluable suggestions and discussions on the turbulence within and under the canopy. The authors would like to thank Rongqian Yang at the National Centers for Environmental Prediction (NCEP) for his insight into the modified two-stream radiation-transfer scheme. Lindsey Gulden is thanked for editing this paper.

References

Anderson, E. A. (1976), A point energy and mass balance model of a snow cover, *NOAA Tech. Rep. NWS 19*, 150 pp., Off. of Hydrol., Natl. Weather Serv., Silver Spring, Md.

Barnett, T. P., L. Dumenil, U. Schlese, E. Roeckner, and M. Latif (1989), The effect of Eurasian snow cover on regional and global climate variations, *J. Atmos. Sci.*, *46*, 661–685.

Betts, A. K., and J. H. Ball (1997), Albedo over boreal forest, *J. Geophys. Res.*, *102*, 28,901–28,909.

Bonan, G. B. (1996), A land surface model (LSM version 1.0) for ecological, hydrological, and atmospheric studies: Technical description and user's guide, *NCAR Tech. Note NCAR/TN-417+STR*, 150 pp., Natl. Cent. for Atmos. Res., Boulder, Colo.

Bonan, G. B., D. Pollard, and S. L. Thompson (1992), Effects of boreal forest vegetation on global climate, *Nature*, *359*, 716–718.

Bonan, G. B., K. J. Davis, D. B. Fitzjarrald, and H. Neumann (1997), Comparison of the NCAR LSM1 land surface model with BOREAS aspen and jack pine tower fluxes, *J. Geophys. Res.*, *102*, 29,065–29,075.

Bonan, G. B., K. W. Oleson, M. Vertenstein, S. Levis, X. Zeng, Y. Dai, R. E. Dickinson, and Z.-L. Yang (2002), The land surface climatology of the community land model coupled to the NCAR community climate model, *J. Clim.*, *15*, 3123–3149.

Brun, E., P. David, M. Sudul, and G. Brunot (1992), A numerical model to simulate snow cover stratigraphy for operational avalanche forecasting, *J. Glaciol.*, *38*, 13–22.

Brutsaert, W. (1982), *Evaporation Into the Atmosphere: Theory, History, and Applications*, D. Reidel, Norwell, Mass.

Businger, J. A., J. C. Wijngaard, Y. I. Izumi, and E. F. Bradley (1971), Flux-profile relationships in the atmosphere surface layer, *J. Atmos. Sci.*, *28*, 181–189.

Cess, R. D., et al. (1991), Intercomparison of snow-feedback as produced by general circulation models, *Science*, *253*, 888–892.

Chalita, S., and L. H. Treut (1994), The albedo of temperate and boreal forest and the Northern Hemisphere climate: A sensitivity experiment using the LMD GCM, *Clim. Dyn.*, *10*, 231–240.

Chen, J. M., T. A. Balck, and R. S. Adams (1991), Evaluation of hemispherical photography for determining plant area index and geometry of a forest stand, *Agric. For. Meteorol.*, *56*, 129–143.

Choudury, B. J., and J. L. Monteith (1988), A four-layer model for the heat budget of homogeneous land surface, *Q. J. R. Meteorol. Soc.*, *114*, 373–398.

Dai, Y., et al. (2003), The Common Land Model (CLM), *Bull. Am. Meteorol. Soc.*, *84*(8), 1013–1023.

Davis, R. E., J. P. Hardy, W. Ni, C. Woodcock, J. C. McKenzie, R. Jordan, and X. Li (1997), Variation of snow cover ablation in the boreal forest: A sensitivity study on the effects of conifer canopy, *J. Geophys. Res.*, *102*, 29,389–29,385.

Deardorff, J. W. (1978), Efficient prediction of ground surface-temperature and moisture, with inclusion of a layer of vegetation, *J. Geophys. Res.*, *83*, 1889–1903.

Dickinson, R. E. (1983), Land surface processes and climate-surface albedos and energy balance, in *Theory of Climate, Adv. Geophys.*, vol. 25, edited by B. Saltzman, pp. 305–353, Academic, San Diego, Calif.

Douville, H., and J. F. Royer (1997), Influence of the temperate and boreal forests on the Northern Hemisphere climate in the Meteo-France climate model, *Clim. Dyn.*, *13*, 57–74.

Douville, H., J. F. Royer, and J. F. Mahfouf (1995), A new snow parameterization for the Meteo-France climate model, part I: Validation in stand-alone experiments, *Clim. Dyn.*, *12*, 21–35.

Essery, R., J. Pomeroy, J. Parviainen, and P. Storck (2003), Sublimation of snow from coniferous forests in a climate model, *J. Clim.*, *16*(11), 1855–1864.

Goudriaan, J. (1977), *Crop Micrometeorology: A Simulation Study*, 257 pp., Pudoc, Wageningen, Netherlands.

Gusev, Y. M., and O. N. Nasonova (2003), The simulation of heat and water exchange in the boreal spruce forest by the land-surface model SWAP, *J. Hydrol.*, *280*, 162–191.

Hardy, J. P., R. E. Davis, R. Jordan, X. Li, C. Woodcock, W. Ni, and J. C. McKenzie (1997), Snow ablation modeling at the stand scale in a boreal jack pine forest, *J. Geophys. Res.*, *102*, 29,397–29,405.

Hedstrom, N. R., and J. W. Pomeroy (1998), Measurements and modeling of snow interception in the boreal forest, *Hydrol. Proc.*, *12*, 1611–1625.

Jordan, R. (1991), A one-dimensional temperature model for a snow cover, *Spec. Rep. 91-16*, Cold Reg. Res. and Eng. Lab., U.S. Army Corps of Eng., Hanover, N. H.

Katul, G. G., and J. D. Albertson (1998), An investigation of higher order closure models for forested canopy, *Boundary-Layer Meteorol.*, *89*, 47–74.

Li, X., A. H. Strahler, and C. R. Woodcock (1995), A hybrid geometric optical and radiative transfer approach for modeling albedo and directional reflectance of discontinuous canopies, *IEEE Trans. Geosci. Remote Sens.*, *33*(2), 466–480.

Link, T. E., and D. Marks (1999), Point simulation of seasonal snow cover dynamics beneath boreal forest canopies, *J. Geophys. Res.*, *104*, 27,841–27,857.

Loth, B., H.-F. Graf, and J. M. Oberhuber (1993), Snow cover model for global climate simulations, *J. Geophys. Res.*, *98*, 10,451–10,464.

Lynch-Stieglitz, M. (1994), The development and validation of a simple snow model for the GISS GCM, *J. Clim.*, *7*, 1842–1855.

Myneni, R. B., R. R. Nemani, and S. W. Running (1997), Estimation of global leaf area index and absorbed par using radiative transfer models, *IEEE Trans. Geosci. Remote Sens.*, *35*, 1380–1393.

Ni, W., X. Li, and C. Woodcock (1997), Transmission of solar radiation in boreal forest conifer forests: Measurements and models, *J. Geophys. Res.*, *102*, 29,555–29,566.

Nijssen, B., and D. Lettenmaier (1999), A simplified approach for predicting shortwave radiation transfer through boreal forest canopies, *J. Geophys. Res.*, *104*(D22), 27,859–27,868.

Poggi, D., A. Porporato, and L. Ridolfi (2004), The effect of vegetation density on canopy sub-layer turbulence, *Boundary-Layer Meteorol.*, *111*, 565–587.

Pomeroy, J. W., and R. A. Schmidt (1993), The use of fractal geometry in modeling and intercepted snow accumulation and sublimation, *Proc. Eastern Snow Conf.*, *50*, 1–10.

Randall, D. A., et al. (1994), Analysis of snow feedbacks in 14 general circulation models, *J. Geophys. Res.*, *99*, 20,757–20,771.

Raupach, M. R., J. J. Finnigan, and Y. Brunt (1996), Coherent eddies and turbulence in vegetation canopies: The mixing layer analogy, *Boundary-Layer Meteorol.*, *78*, 351–382.

Roesch, A., M. Wild, H. Gilgen, and A. Ohmura (2001), A new snow cover fraction parameterization for ECHAM4 GCM, *Clim. Dyn.*, *17*, 933–946.

Schmidt, R. A., and D. R. Gluns (1991), Snowfall interception on branches of three conifer species, *Can. J. For. Res.*, *21*, 1262–1269.

Sellers, P. J. (1985), Canopy reflectance, photosynthesis and transpiration, *Int. J. Remote Sens.*, *6*, 1335–1372.

Sellers, P. J., Y. Mintz, Y. C. Sud, and A. Dalcher (1986), A simple biosphere model (SIB) for use within general-circulation models, *J Atmos. Sci.*, *43*, 505–531.

Sellers, P. J., et al. (1997), BOREAS in 1997: Experiment overview, scientific results, and future directions, *J. Geophys. Res.*, *102*, 28,731–28,769.

Shaw, R. H., and E. G. Patton (2003), Canopy element influences on resolved- and subgrid-scale energy within a large-eddy simulation, *Agric. For. Meteorol.*, *115*, 5–17.

Shewchuk, S. R. (1997), Surface mesonet for BOREAS, *J. Geophys. Res.*, *102*, 29,077–29,082.

Shuttleworth, W. J., and J. S. Wallace (1985), Evaporation from sparse crops-an energy combination theory, *Q. J. R. Meteorol. Soc.*, *111*, 839–855.

Storck, P., and D. P. Lettenmaier (2000), Trees, snow and flooding: An investigation of forest canopy effects on snow accumulation and melt at the plot and watershed scales in the Pacific Northwest, *Water Resour. Ser. Tech. Rep. 161*, 176 pp., Univ. of Wash., Seattle, Wash. (Available at http://www.ce.washington.edu/pub/lettenmaier/WRS161.pdf.)

Storck, P., D. P. Lettenmaier, and S. M. Bolton (2002), Measurement of snow interception and canopy effects on snow accumulation and melt in a mountainous maritime climate, Oregon, United States, *Water Resour. Res.*, *38*(11), 1223, doi:10.1029/2002WR001281.

Sun, S. F., J. M. Jin, and Y. Xue (1999), A simple Snow-Atmosphere-Soil Transfer (SAST) model, *J. Geophys. Res.*, *104*, 19,587–19,597.

Thomas, G., and P. R. Rowntree (1992), The boreal forests and climate, *Q. J. R. Meteorol. Soc.*, *118*, 469–497.

Tian, Y., et al. (2004), Comparison of seasonal and spatial variations of leaf area index and fraction of absorbed photosynthetically active radiation from Moderate Resolution Imaging Spectroradiometer (MODIS) and Common Land Model, *J. Geophys. Res.*, *109*, D01103, doi:10.1029/2003JD003777.

Verseghy, D. L. (1991), CLASS—A Canadian Land Surface Scheme for GCMs, part I: Soil model, *Int. J. Climatol.*, *11*, 111–133.

Walsh, J. E., and B. Ross (1988), Sensitivity of 30-day dynamical forecast to continental snow cover, *J. Clim.*, *1*, 739–754.

Xue, Y., S. Sun, D. S. Kahan, and Y. Jiao (2003), Impact of parameterizations in snow physics and interface processes on the simulation of snow cover and runoff at several cold region sites, *J. Geophys. Res.*, *108*(D22), 8859, doi:10.1029/2002JD003174.

Yang, R., and M. A. Friedl (2003), Modeling the effects of three-dimensional vegetation structure on surface radiation and energy balance in boreal forests, *J. Geophys. Res.*, *108*(D16), 8615, doi:10.1029/2002JD003109.

Yang, R., M. Friedl, and W. Ni (2001), Parameterization of shortwave radiation fluxes for nonuniform vegetation canopies in land surface models, *J. Geophys. Res.*, *106*, 14,275–14,286.

Yang, Z.-L., and G.-Y. Niu (2003), The versatile integrator of surface and atmosphere processes (VISA) part I: Model description, *Global Planet. Change*, *38*, 175–189.

Yang, Z.-L., R. E. Dickinson, A. Robock, and K. Y. Vinnikov (1997), Validation of the snow sub-model of the biosphere-atmosphere transfer scheme with Russian snow cover and meteorological observational data, *J. Clim.*, *10*, 353–373.

Yeh, T.-C., R. T. Wetherald, and Manabe (1983), A model study of the short-term climate and hydrologic effects of sudden snow-cover removal, *Mon. Weather Rev.*, *111*, 1013–1024.

Zeng, X., M. Shaikh, Y. Dai, R. E. Dickinson, and R. Myneni (2002), Coupling of the common land model to the NCAR community climate model, *J. Clim.*, *15*, 1832–1854.

Zhou, L., et al. (2003), Comparison of seasonal and spatial variations of albedos from Moderate-Resolution Imaging Spectroradiometer (MODIS) and Common Land Model, *J. Geophys. Res.*, *108*(D15), 4488, doi:10.1029/2002JD003326.

G.-Y. Niu and Z.-L. Yang, Department of Geological Sciences, John A. and Katherine G. Jackson School of Geosciences, University of Texas at Austin, Austin, TX 78712-0254, USA. (niu@geo.utexas.edu)